

Majorization-Minimization Networks for Inverse Problems: An Application to EEG Imaging

Le Minh Triet Tran, Sarah Reynaud, Ronan Fablet, Adrien Merlini, François Rousseau, and Mai Quyen Pham

Abstract

Inverse problems are often ill-posed and require optimization schemes with strong stability and convergence guarantees. While learning-based approaches such as deep unrolling and meta-learning achieve strong empirical performance, they typically lack explicit control over descent and curvature, limiting robustness. We propose a learned Majorization-Minimization (MM) framework for inverse problems within a bilevel optimization setting. Instead of learning a full optimizer, we learn a structured curvature majorant that governs each MM step while preserving classical MM descent guarantees. The majorant is parameterized by a lightweight recurrent neural network and explicitly constrained to satisfy valid MM conditions. For cosine-similarity losses, we derive explicit curvature bounds yielding diagonal majorants. When analytic bounds are unavailable, we rely on efficient Hessian-vector product-based spectral estimation to automatically upper-bound local curvature without forming the Hessian explicitly. Experiments on EEG source imaging demonstrate improved accuracy, stability, and cross-dataset generalization over deep-unrolled and meta-learning baselines.

Index Terms

Bilevel Optimization, Learned Majorization-Minimization, Recurrent Neural Networks, EEG Source Imaging.

I. INTRODUCTION

ESTIMATING a phenomenon from indirect or noisy measurements leads to an inverse problem, which is typically ill-posed and requires appropriate priors to ensure stable recovery [1]. Such problems arise in numerous applications, including imaging, geoscience, and biomedical signal analysis, and are particularly challenging in EEG source imaging (ESI), where one aims to infer cortical activity from scalp measurements through an ill-conditioned forward model and highly noisy observations [2]–[4]. In practice, the choice of an appropriate regularization is highly problem-dependent, often requiring substantial manual tuning and expert knowledge. This difficulty has motivated the development of learning-based approaches that infer priors or optimization strategies directly from data.

Modern learning-based approaches increasingly rely on deep priors or unrolled iterative schemes, where a fixed number of optimization steps is made differentiable and trained end-to-end [5]–[10]. While these methods often achieve strong empirical performance, they remain sensitive to the choice of inner solvers and step sizes, and offer limited control over convergence and stability. Moreover, after training, the unrolled updates typically deviate from their original optimization interpretation, which reduces interpretability and makes convergence guarantees difficult to establish.

In parallel, Learning-to-Learn (L2L) and meta-learning strategies aim to learn the optimization process itself, either by training neural networks to generate update rules [11], [12] or by learning geometric transformations of gradients, such as Meta-Curvature [13] or ModGrad [14], often within the Model Agnostic Meta Learning (MAML) framework [15]. While these approaches demonstrate the potential of data-driven optimization, they typically do not provide explicit theoretical guarantees, such as descent or majorization properties. This lack of analytical structure makes their behavior harder to interpret and complicates the analysis of robustness in ill-posed inverse problems.

To address these limitations, we introduce a learned Majorization-Minimization (MM) solver, formulated within a bilevel optimization framework. MM algorithms rely on the construction of quadratic surrogate majorants whose minimizers guarantee descent [16], thereby providing a principled, interpretable, and stable update mechanism. Rather than learning an optimizer end-to-end, we preserve the analytical structure of gradient-based MM iterations and learn only the curvature majorant that controls each update. This curvature majorant is parameterized by recurrent neural networks (RNNs) that adapt dynamically to the current state and its gradient, effectively combining the explicit theoretical guarantees and analytical structure of classical MM methods with the adaptability of meta-learning.

A central theoretical contribution of this work is the derivation of explicit curvature bounds for cosine-similarity losses, which are widely used in inverse problems and learned regularization. These bounds lead to simple diagonal quadratic majorants and provide closed-form conditions under which MM updates remain valid, even in the presence of nonlinear learned representations.

This work was supported by the European Innovation Council (EIC) through the European Union's Horizon Europe research Programme under Grant 101046748 (Project CEREBRO). This work was granted access to the HPC resources of IDRIS under the allocation 2023-AD010314332 made by GENCI.

Le Minh Triet Tran (corresponding author), Sarah Reynaud, and François Rousseau are with *IMT Atlantique, LaTIM U1101 INSERM*, Brest, France (emails: {le-minh-triet.tran, sarah.reynaud, francois.rousseau}@imt-atlantique.fr).

Ronan Fablet, Adrien Merlini, and Mai Quyen Pham are with *IMT Atlantique, Lab-STICC UMR CNRS 6285*, Brest, France (emails: {ronan.fablet, adrien.merlini, mai-quyen.pham}@imt-atlantique.fr).

When analytic curvature bounds are unavailable or impractical, we propose an automatic curvature estimation strategy that enables the construction of valid MM majorants for complex losses, while preserving theoretical soundness.

Together, these contributions yield a learned MM solver whose lower-level iterates admit provable descent and convergence guarantees under the derived curvature conditions. When embedded into the bilevel formulation, this stability ensures that the overall learning process satisfies the standard assumptions required for convergence to stationary points in nonconvex bilevel optimization, as characterized in [17], [18]. We demonstrate the practical impact of these guarantees on ESI, where the proposed method consistently outperforms deep-unrolled and meta-learning baselines, providing improved stability, faster convergence, and more accurate reconstructions. Overall, the results highlight learned MM solver as a powerful and theoretically grounded paradigm for inverse-problem optimization.

The paper is organized as follows. Section II reviews related work. Section III formulates the ill-posed inverse problem studied in this paper and recalls the main principles and conditions of quadratic MM. The proposed methodology is presented in Sections IV and V. In Section IV, we address the construction of valid quadratic MM majorants for cosine-similarity losses with analytical upper bounds, as well as for general twice-differentiable losses with Lipschitz-continuous gradients. Section V then introduces the bilevel optimization framework based on the proposed MM solver. Section VI describes the application setting and datasets. Section VII reports experimental results on the ESI problem. Finally, Section VIII concludes the paper and outlines directions for future work.

Notation: Uppercase bold letters (e.g., \mathbf{L}) denote matrices, and lowercase bold letters (e.g., \mathbf{x}) denote column vectors. The symbol \odot denotes the Hadamard (entry-wise) product. $\text{Diag}(\mathbf{v})$ denotes the diagonal matrix with entries defined from vector \mathbf{v} . $\mathbf{D} \succeq 0$ (resp. $\mathbf{D} \succ 0$) means that $\mathbf{D} \in \mathbb{R}^{n \times n}$ is positive semi-definite, SPD (resp. positive definite, PD), that is, for all $\mathbf{x} \in \mathbb{R}^n$, $\mathbf{x}^\top \mathbf{D} \mathbf{x} \geq 0$ (resp. $\mathbf{x}^\top \mathbf{D} \mathbf{x} > 0$). $\mathbf{1}_n$ denotes the vector of ones with length n and $\mathbf{1}_{m,n} = \mathbf{1}_m \mathbf{1}_n^\top$.

II. RELATED WORKS

Classical inverse problems are commonly addressed using regularized optimization, typically through gradient-based or proximal algorithms. Within this landscape, MM offers a principled way to guarantee monotone descent by minimizing tractable surrogate upper bounds of the objective [16], and includes the Expectation Maximization (EM) algorithm as a special case [19]. MM has been widely used in imaging, notably through iteratively reweighted least squares [20], half-quadratic splitting [21], and variational surrogate methods [22]. However, constructing quadratic majorants requires hand-designed curvature bounds tailored to each loss and forward operator, which limits the applicability of classical MM to modern settings with nonlinear learned representations. Existing MM formulations rely on fixed analytic majorants, to our knowledge, none learns a structured curvature majorant while retaining MM descent guarantees.

Deep unrolling provides a data-driven alternative by truncating iterative algorithms and training them end-to-end [5]–[10]. These architectures hard-wire the structure of classical solvers while allowing certain parameters to be learned from data, such as thresholds, step sizes, or proximal operators. Although this often yields significant empirical gains, the learned parameters are no longer tied to analytic surrogate functions or curvature models. As a result, the resulting updates generally cannot be interpreted as MM steps nor linked to any implicit majorant, limiting insight into the underlying optimization geometry and stability.

Preconditioning is another strategy to improve convergence and robustness in ill-posed problems. Traditional approaches range from diagonal scalings such as the Jacobi method to more sophisticated techniques including incomplete Cholesky factorizations and preconditioned conjugate-gradient methods [23], [24]. Newton’s method may be viewed as an ideal form of preconditioning through the inverse Hessian, though its computational cost motivates quasi-Newton variants such as BFGS and L-BFGS [25]. In machine learning, adaptive gradient methods such as AdaGrad, RMSProp, and Adam [26], [27] can similarly be interpreted as learning diagonal preconditioners from gradient statistics. Despite their effectiveness, these methods are not derived from a surrogate-based or majorization principle and thus lie outside the MM framework.

L2L and meta-learning approaches aim to learn the optimization process itself, either through neural update rules [11], [12], geometry-aware gradient transformations [13], [14], or more recent designs such as greedy learned optimizers [28] and transformer-based preconditioning models [29]. While highly flexible, these optimizer-centric methods typically lack the structure required to enforce or analyze monotonicity and descent properties, which limits their applicability to severely ill-posed inverse problems.

Several recent works have also incorporated neural networks into MM-inspired procedures, for example by learning proximal operators [30]–[33] or by unfolding half-quadratic [34] and ADMM-based schemes [6]. However, these approaches replace rather than preserve the MM principle: their learned updates do not explicitly enforce surrogate validity, curvature control, or descent guarantees and therefore depart from the classical MM framework.

Take together, these limitations highlight the need for optimization schemes that preserve the theoretical guarantees of MM while adapting to data through learning. Bridging this gap, by learning structured curvature majorants without sacrificing interpretability or stability, remains largely unexplored and forms the foundation of the learned MM framework proposed in this work.

III. PRELIMINARIES

A. Problem Setup

When solving inverse problems, the goal is to estimate an unknown signal $\mathbf{x} \in \mathbb{R}^s$ from measurements $\mathbf{y} \in \mathbb{R}^n$ through an observation model

$$\mathbf{y} = \mathbf{L}\mathbf{x} + \boldsymbol{\varepsilon}, \quad (1)$$

where $\boldsymbol{\varepsilon} \in \mathbb{R}^n$ represents measurement noise or modeling error, and $\mathbf{L} \in \mathbb{R}^{n \times s}$ is a linear forward operator defining the observation model. In practice, \mathbf{L} is often non-invertible (typically $s > n$) and highly sensitive to noise, making (1) an ill-posed problem.

In order to stable the problem numerically, without loss of generally we can assume that measurements have a non-zero energy and this is bounded. That means there exists two constants $\bar{\delta} \geq \underline{\delta} > 0$ such that $\mathbf{y} \in \mathcal{C} = \{\mathbf{y} \in \mathbb{R}^n : \underline{\delta} \leq \|\mathbf{y}\| \leq \bar{\delta}\}$.

The unknown signal \mathbf{x} can estimated by solving a regularized variational problem of the form

$$\hat{\mathbf{x}}(\boldsymbol{\theta}) = \arg \min_{\mathbf{x} \in \mathbb{R}^s} u(\mathbf{x}; \mathbf{y}, \boldsymbol{\theta}) = f(\mathbf{y}, \mathbf{L}\mathbf{x}) + \lambda h(\Phi(\mathbf{x}; \boldsymbol{\theta})), \quad (2)$$

where the objective combines a data-fidelity term and a learned regularization term. This formulation follows the standard strategy in inverse problems of stabilizing an ill-posed reconstruction through the use of appropriate prior information.

To mirror the classical structure used in inverse problems, the cost function is decomposed into two components:

- **Data fidelity**

The function $f : \mathbb{R}^n \times \mathbb{R}^s \rightarrow \mathbb{R}$ measures the discrepancy between the measurements \mathbf{y} and their reconstruction $\mathbf{L}\mathbf{x}$. We assume that f is a twice differentiable with a μ_f -Lipschitz gradient.¹

- **Regularization**

The prior is encoded through the composition $h(\Phi(\mathbf{x}; \boldsymbol{\theta}))$ where

$\Phi : \mathbb{R}^s \rightarrow \mathbb{R}^m$ is a (possibly nonlinear) representation operator, twice differentiable and parameterized by $\boldsymbol{\theta}$, and

$h : \mathbb{R}^m \rightarrow \mathbb{R}$ is a differentiable function promoting desirable properties in the recovered sources. We assume that h has a μ_h -Lipschitz continuous gradient.

- **Trade-off parameter**

The scalar $\lambda > 0$ balances data fidelity against the regularization term.

This framework captures a broad class of regularized inverse problems, where the choices of f , the representation Φ , the prior h , and the regularization weight λ crucially influence the recovered solution. As widely documented [9], [35], [36], selecting these components, particularly designing an effective representation Φ or tuning λ , remains a central challenge, as these choices are highly problem-dependent and sensitive to both the data and the application at hand.

We propose to compute $\hat{\mathbf{x}}(\boldsymbol{\theta})$ via an iterative solver that generates a sequence $\hat{\mathbf{x}}^0(\boldsymbol{\theta}), \hat{\mathbf{x}}^1(\boldsymbol{\theta}), \dots$. This solver is based on a MM strategy.

B. Quadratic MM and Majorant Condition

MM methods solve a minimization problem by iteratively replacing a difficult function with a simpler upper-bounding surrogate. Here we construct a quadratic majorant of the objective in (2). We recall the definition below.

Definition 1. Let $\xi : \mathbb{R}^s \rightarrow \mathbb{R}$ be a differentiable function, and let $\bar{\mathbf{x}} \in \mathbb{R}^s$ be a reference point. For any $\mathbf{x} \in \mathbb{R}^s$, define the quadratic surrogate

$$Q(\mathbf{x}, \bar{\mathbf{x}}) = \xi(\bar{\mathbf{x}}) + (\mathbf{x} - \bar{\mathbf{x}})^\top \nabla \xi(\bar{\mathbf{x}}) + \frac{1}{2}(\mathbf{x} - \bar{\mathbf{x}})^\top \mathbf{P}_{\bar{\mathbf{x}}}(\mathbf{x} - \bar{\mathbf{x}}), \quad (3)$$

where $\mathbf{P}_{\bar{\mathbf{x}}} \in \mathbb{R}^{s \times s}$ is a symmetric positive definite (SPD) matrix. The matrix $\mathbf{P}_{\bar{\mathbf{x}}}$ is said to satisfy the majorant condition at $\bar{\mathbf{x}}$ if

$$\xi(\mathbf{x}) \leq Q(\mathbf{x}, \bar{\mathbf{x}}), \quad \forall \mathbf{x} \in \mathbb{R}^s. \quad (4)$$

In this case, $Q(\cdot, \bar{\mathbf{x}})$ is a quadratic majorant of ξ at $\bar{\mathbf{x}}$.

Since $\mathbf{P}_{\bar{\mathbf{x}}}$ is SPD, minimizing the quadratic surrogate yields a closed-form update:

$$\hat{\mathbf{x}} = \bar{\mathbf{x}} - \mathbf{P}_{\bar{\mathbf{x}}}^{-1} \nabla \xi(\bar{\mathbf{x}}). \quad (5)$$

A key benefit of MM is that the majorant can provide a larger and safer descent step than standard gradient descent. However, using a dense SPD matrix requires computing $\mathbf{P}_{\bar{\mathbf{x}}}^{-1}$, which may be computationally expensive.

To balance computational efficiency and convergence guarantees (i.e. ensuring $\mathbf{P}_{\bar{\mathbf{x}}}$ closely upper-bounds the Hessian matrix), we aim to construct a *diagonal* majorant matrix $\mathbf{P}_{\bar{\mathbf{x}}}$, which allows for fast inversion while satisfying the majorization condition. Since the MM update involves only the inverse majorant, we write $\mathbf{P}_{\bar{\mathbf{x}}}^{-1} = \text{Diag}(\mathbf{p})$, where $\mathbf{p} \in \mathbb{R}^s$ denotes the vector of inverse diagonal curvature coefficients, thus $\mathbf{P}_{\bar{\mathbf{x}}}^{-1} \nabla \xi(\bar{\mathbf{x}}) = \mathbf{p} \odot \nabla \xi(\bar{\mathbf{x}})$.

¹A twice differentiable function f is a μ -Lipschitz gradient if there exists a constant $\mu < +\infty$ such that $\|\nabla f(\mathbf{x}) - \nabla f(\mathbf{y})\| \leq \mu \|\mathbf{x} - \mathbf{y}\|$, $\forall \mathbf{x}, \mathbf{y} \in \mathbb{R}^n$.

IV. LEARNING A CONVERGENT MM SOLVER

Gradient-Lipschitz bounds for classical loss functions, such as the squared ℓ_2 (MSE) loss, the ℓ_1 loss associated with Laplace noise, or the KL divergence, are well established in the optimization literature [37]–[39]. In contrast, to our knowledge, no standard Lipschitz gradient bounds are available for the cosine similarity, despite its increasing importance in applications where scale and amplitude invariance are desirable, such as ESI. This limitation becomes problematic when cosine similarity is incorporated into iterative optimization schemes, for example in MM, since explicit curvature bounds are required to construct a valid quadratic majorant.

In what follows, we derive explicit diagonal upper bounds on the Hessian of the cosine similarity, which yield a computable Lipschitz constant for its gradient and allow the integration of cosine similarity into MM-based solvers with convergence guarantees.

A. MM solver for Cosine Similarity

We consider the cosine similarity between two vectors $\mathbf{a} \in \mathbb{R}^{*s}$ and $\mathbf{b} \in \mathbb{R}^{*s}$, defined as

$$S_C(\mathbf{a}, \mathbf{b}) = \frac{\mathbf{a}^\top \mathbf{b}}{\|\mathbf{a}\| \|\mathbf{b}\|}. \quad (6)$$

Note that when working with cosine similarity, we implicitly constrain the admissible solutions so that the measure is well defined. In particular, we assume the existence of a small constant $v > 0$ such that $\mathbf{x} \in \mathcal{D} = \{\mathbf{x} \in \mathbb{R}^s : \|\mathbf{x}\| \geq v\}$. This assumption is mild and does not restrict the applicability of our model. In ESI, the goal is to recover non-vanishing cortical activations from noisy observations. Even when no true source is active, the measurement process introduces a nonzero noise floor. Consequently, iterates produced by practical solvers rarely approach the zero vector, and the v -constraint simply formalizes a condition that naturally holds in realistic scenarios.

Under this assumption, together with the bounded energy of the observation data, we show that the cosine similarity loss has a Lipschitz continuous gradient on any bounded convex subset of \mathcal{D} . This property is desirable for designing efficient algorithms to minimize the loss. The proof is provided in Appendix A and B.

The following Proposition states the conditions that ensure the construction of a valid MM function when using S_C as the similarity measure for the different terms of the loss in Problem 2.

Proposition 1. *For every $\mathbf{x}(\boldsymbol{\theta}) \in \mathbb{R}^s$, $\mathbf{y} \in \mathbb{R}^n$, and $\mathbf{L} \in \mathbb{R}^{n \times s}$, define the vector $\mathbf{p}(\mathbf{x}(\boldsymbol{\theta})) \in \mathbb{R}^s$ such that*

$$\underline{\nu} \mathbf{1} \preceq \mathbf{p}(\mathbf{x}(\boldsymbol{\theta})) \preceq \frac{1}{\mu_1 + \lambda \mu_2} \mathbf{1}, \quad (7)$$

where $\underline{\nu} > 0$, $\mu_1 = 5 \frac{\|\mathbf{L}\|^2}{\|\mathbf{L}\mathbf{x}\|^2}$, and

$$\mu_2 = \frac{1}{\beta \|\mathbf{x}\|} (5\varrho + 1) + \frac{2\alpha\sqrt{s}}{\beta} + 4 \left(\frac{\varrho}{\beta} + \frac{1}{\|\mathbf{x}\|} \right)^2$$

$$\text{with } \varrho = \|\nabla_{\mathbf{x}} \Phi(\mathbf{x}; \boldsymbol{\theta})\|, \\ \alpha = \max_{1 \leq i \leq s} \|\nabla_{\mathbf{x}}^2 [\Phi(\mathbf{x}; \boldsymbol{\theta})]_i\|, \quad \beta = \|\Phi(\mathbf{x}; \boldsymbol{\theta})\|.$$

If there exist $0 < \underline{\varrho} < \bar{\varrho} < +\infty$ such that $\alpha, \rho < \bar{\varrho}$ and $\underline{\varrho} < \beta < \bar{\varrho}$, then, $\mathbf{p}(\mathbf{x}(\boldsymbol{\theta}))$ satisfies the majorization condition for the loss function of 2 when using the cosine similarity measure.

Proof. The proof of this Proposition is provided in Appendix A. □

B. MM solver for a twice differentiable and gradient Lipschitz loss function

While we have provided analytic curvature bounds for cosine-similarity-based loss function, such closed-form derivations may become intractable when the loss or the representation operator $\Phi_{\boldsymbol{\theta}}$ becomes extremely complex. In these settings, it is desirable to estimate the local bounds automatically so that the constraints required by the learned solver can still be enforced. To this end, we introduce a power-iteration-based procedure that computes a numerical estimate of the dominant eigenvalue of the Hessian, thereby providing an automatic upper bound on the local curvature. Indeed, the tightest local upper bound of a twice-differentiable loss is the spectral norm of its Hessian:

$$\|\nabla^2 u(\mathbf{x}; \mathbf{y}, \boldsymbol{\theta})\| = \lambda_{\max}(\nabla^2 u(\mathbf{x}; \mathbf{y}, \boldsymbol{\theta})),$$

which quantifies the worst-case quadratic expansion of u around \mathbf{x} [37], [38]. By the Rayleigh–Ritz theorem,

$$\lambda_{\max} = \max_{\|\mathbf{v}\|=1} \mathbf{v}^\top (\nabla^2 u(\mathbf{x}; \mathbf{y}, \boldsymbol{\theta})) \mathbf{v}, \quad (8)$$

so estimating the dominant eigenvalue λ_{\max} is equivalent to identifying this fundamental smoothness constant.

Since the gradient $\nabla u(\mathbf{x}; \mathbf{y}, \boldsymbol{\theta})$ is already computed during the backward pass of the lower-level optimization, HVPs can be obtained efficiently without forming the Hessian explicitly. Indeed, $\forall \mathbf{v} \in \mathbb{R}^s$, the identity

$$\nabla(\nabla u(\mathbf{x}; \mathbf{y}, \boldsymbol{\theta})^\top \mathbf{v}) = \nabla^2 u(\mathbf{x}; \mathbf{y}, \boldsymbol{\theta}) \mathbf{v}$$

allows evaluating $\nabla^2 u(\mathbf{x}; \mathbf{y}, \boldsymbol{\theta}) \mathbf{v}$ via a single reverse-mode automatic differentiation, following Pearlmutter's method [40]. Leveraging this, power iteration provides an efficient mechanism to approximate λ_{\max} . Starting from a random unit vector \mathbf{v}_0 , the normalized iteration,

$$\mathbf{v}_{k+1} = \frac{\nabla^2 u(\mathbf{x}; \mathbf{y}, \boldsymbol{\theta}) \mathbf{v}_k}{\|\nabla^2 u(\mathbf{x}; \mathbf{y}, \boldsymbol{\theta}) \mathbf{v}_k\|}$$

converges under mild assumptions to the dominant eigenvector \mathbf{v} , while the Rayleigh quotient $\mathbf{v}_k^\top \nabla^2 u(\mathbf{x}; \mathbf{y}, \boldsymbol{\theta}) \mathbf{v}_k$ converges geometrically to λ_{\max} [41]. In practice, this procedure is implemented using standard automatic differentiation tools to compute HVPs, but avoids computing or storing the full Hessian explicitly, making it well suited to high-dimensional inverse problems. The resulting bound-estimation algorithm is summarized in Algorithm 1.

Algorithm 1 Hessian Spectral Norm Estimation via Power Iteration

Input: gradient $\nabla u(\mathbf{x}; \mathbf{y}, \boldsymbol{\theta})$, state \mathbf{x} , and iterations K .

Init: Sample $\mathbf{v}_0 \sim \mathcal{N}(0, \mathbf{I})$, normalize $\mathbf{v}_0 \leftarrow \mathbf{v}_0 / \|\mathbf{v}_0\|$

Output: $\hat{\mathbf{v}}$ and $\hat{\lambda}_{\max}$.

```

1: for  $k = 0$  to  $K - 1$  do
2:    $\mathbf{u}_k = \nabla(\nabla u(\mathbf{x}; \mathbf{y}, \boldsymbol{\theta})^\top \mathbf{v}_k)$  (HVP via autodiff)
3:    $\mathbf{v}_{k+1} = \mathbf{u}_k / \|\mathbf{u}_k\|$ 
4: end for
5:  $\hat{\lambda}_{\max} = \mathbf{v}_K^\top \nabla(\nabla u(\mathbf{x}; \mathbf{y}, \boldsymbol{\theta})^\top \mathbf{v}_K)$ 
6: return  $\hat{\mathbf{v}} = \mathbf{v}_K$ ,  $\hat{\lambda}_{\max}$ 

```

V. BILEVEL OPTIMIZATION WITH MM-BASED SOLVER

A. Bilevel optimization

In this work, we focus on the use of bilevel approaches to solve inverse problems (1). We adopt the framework proposed in [3], which employs an AutoEncoder (AE) architecture to learn appropriate characteristics of the signal of interest. This representation is then integrated into the regularization term, leading to a supervised bilevel optimization formulation for solving the inverse problem. Therefore the supervised problem can be formulated as a bilevel optimization problem [36], [42]

$$\hat{\boldsymbol{\theta}} = \arg \min_{\boldsymbol{\theta}} \mathbb{E}[\ell(\mathbf{x}, \hat{\mathbf{x}}(\boldsymbol{\theta}))] \quad (9a)$$

$$\text{s.t. } \hat{\mathbf{x}}(\boldsymbol{\theta}) = \arg \min_{\mathbf{x}} u(\mathbf{x}; \mathbf{y}, \boldsymbol{\theta}), \quad (9b)$$

where (\mathbf{x}, \mathbf{y}) be a set of training data which satisfies (1). The Eq. (9b) is called the lower-level and estimates $\hat{\mathbf{x}}(\boldsymbol{\theta})$ as the solution of a variational optimization problem while (9a) is called the upper-level and trains the neural network with loss function ℓ between the ground truth \mathbf{x} and the estimate of lower-level problem $\hat{\mathbf{x}}(\boldsymbol{\theta})$.

Algorithm 2 Bilevel optimization algorithm

Input: training set $(\mathbf{x}, \mathbf{y}, \mathbf{L})$, let $I, J \in \mathbb{N}^*$, and let $0 < \gamma < 2$.

Initializations: set $\mathbf{x}^0 \in \text{dom } u$ and $\boldsymbol{\theta}^0 \in \text{dom } \ell$

Output: $\boldsymbol{\theta}^J$

```

1: for  $j = 0$  to  $J - 1$  do
2:   for  $i = 0$  to  $I - 1$  do
3:     #lower-solver
4:      $\mathbf{x}^{i+1}(\boldsymbol{\theta}^j) = \mathbf{x}^i(\boldsymbol{\theta}^j) - \gamma \mathbf{p}(\mathbf{x}^i(\boldsymbol{\theta}^j), \mathbf{g}^i) \odot \mathbf{g}^i$ 
5:   end for
6:    $\hat{\mathbf{x}}(\boldsymbol{\theta}^j) = \mathbf{x}^I(\boldsymbol{\theta}^j)$ 
7:   #upper-solver
8:    $\boldsymbol{\theta}^{j+1} = \arg \min_{\boldsymbol{\theta}} \ell(\mathbf{x}, \hat{\mathbf{x}}(\boldsymbol{\theta}))$ 
9: end for

```

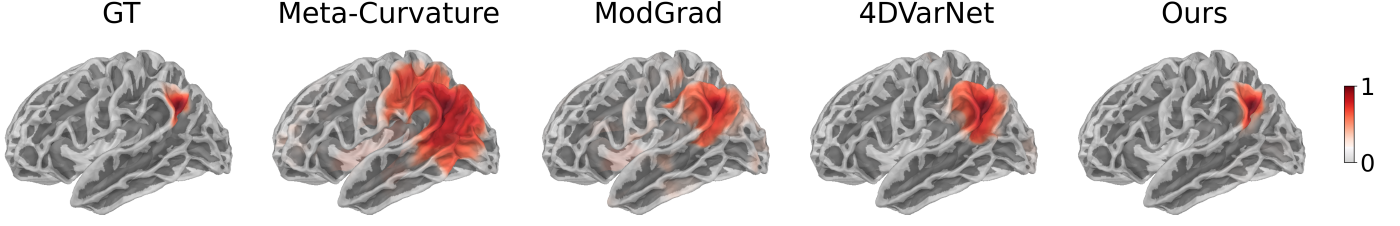


Fig. 1: Visualizing the estimate result of the methods.

Dataset (Train → Eval)	Method	Params (M)	LE ↓	AUC ↑	nMSE ↓	PSNR ↑	TE ↓
SEREEGA → SEREEGA	Meta-Curvature	1.80	10.22	97.86	0.01	27.90	0.72
	ModGrad	1.34	28.68	69.12	0.06	21.54	1.60
	4DVarNet	3.01	9.17	99.52	0.01	30.35	1.04
	Ours	2.95	3.92	99.90	0.00	38.74	0.79
NMM → NMM	Meta-Curvature	2.05	17.58	84.08	0.02	30.39	170.12
	ModGrad	7.11	38.03	64.32	0.02	29.15	196.32
	4DVarNet	3.01	15.13	80.32	0.01	32.68	166.24
	Ours	2.95	9.98	82.41	0.01	35.81	146.24
SEREEGA → NMM	4DVarNet	3.01	14.40	74.97	0.02	30.23	156.44
	Ours	2.95	12.48	75.03	0.01	33.72	133.44
NMM → SEREEGA	4DVarNet	3.01	20.68	92.74	0.02	22.99	1.62
	Ours	2.95	16.74	92.87	0.01	25.64	1.47

TABLE I: Quantitative comparison across four training–evaluation configurations: (i) SEREEGA → SEREEGA, (ii) NMM → NMM, (iii) SEREEGA → NMM, and (iv) NMM → SEREEGA. Best results within each block are highlighted in bold.

The convergence of Algorithm 2 follows from standard results in nonconvex bilevel optimization with inexact inner solvers. In particular, under standard smoothness, boundedness, and step-size conditions, and for a fixed number of inner iterations, the resulting bilevel procedure converges to a stationary point of the upper level objective. This setting falls within the framework analyzed in [43], which establishes convergence to critical points for bilevel problems with truncated gradient based inner solvers.

B. Solver Architecture with Curvature Majorant

Motivated by the limitations of fixed, hand-crafted MM majorants identified in Section II, our objective is to learn a curvature majorant that adapts to the current iterate while provably preserving the MM descent condition. Rather than learning a full optimizer as in meta-learning approaches, we retain the analytical MM update structure and parameterize only the curvature model governing each surrogate step.

At iteration i , let $\mathbf{g}^i = \nabla_{\mathbf{x}} u(\mathbf{x}^i; \mathbf{y}, \boldsymbol{\theta})$ denote the gradient of the variational energy. We predict a diagonal curvature majorant $\tilde{\mathbf{p}}^i = \tilde{\mathbf{p}}(\mathbf{x}^i, \mathbf{g}^i) \in \mathbb{R}^s$ using two recurrent modules:

$$\tilde{\mathbf{p}}(\mathbf{x}^i, \mathbf{g}^i) = \mathcal{F}_1(\mathbf{g}^i; \boldsymbol{\theta}_1) \odot \mathcal{F}_2(\mathbf{x}^i, \mathcal{F}_1(\mathbf{g}^i; \boldsymbol{\theta}_1); \boldsymbol{\theta}_2), \quad (10)$$

where \mathcal{F}_1 extracts gradient-dependent features and \mathcal{F}_2 refines them using the current state. The hidden states of the recurrent modules ensure temporal consistency across iterations. In practice, we instantiate \mathcal{F}_1 and \mathcal{F}_2 using ConvLSTM cells [44], which better exploit spatio-temporal structure and are more compatible with modern deep learning libraries than standard LSTMs in this context. To ensure that the learned majorant satisfies the MM majorization condition, $\tilde{\mathbf{p}}^i$ is projected onto a valid curvature interval:

$$\mathbf{p}^i = \text{proj}_{\mathcal{C}^i}(\tilde{\mathbf{p}}^i), \quad \mathcal{C}^i = \{\mathbf{p} \in \mathbb{R}^s : \underline{\mathbf{1}} \leq \mathbf{p} \leq \bar{\mathbf{1}}\}, \quad (11)$$

where $\text{proj}_{\mathcal{C}^i}$ denotes the Euclidean projection onto the convex set \mathcal{C}^i . The lower bound $\underline{\mathbf{1}} > 0$ enforces positivity of the inverse curvature vector, while the upper bound $\bar{\mathbf{1}}$ encodes a local curvature constraint ensuring that the resulting diagonal matrix defines a valid MM majorant. The value of $\bar{\mathbf{1}}$ is obtained either from closed-form analytic curvature bounds, when available (e.g., for cosine-similarity losses as established in (7)), or from an automatic estimate of the dominant Hessian eigenvalue $\hat{\lambda}_{\max}$ computed using Algorithm 1, by setting $\bar{\mathbf{1}} = 1/\hat{\lambda}_{\max}$.

The resulting vector \mathbf{p}^i induces a valid diagonal quadratic majorant of the loss at \mathbf{x}^i and is used within the MM update rule in (5). The complete bilevel training procedure is summarized in Algorithm 2.

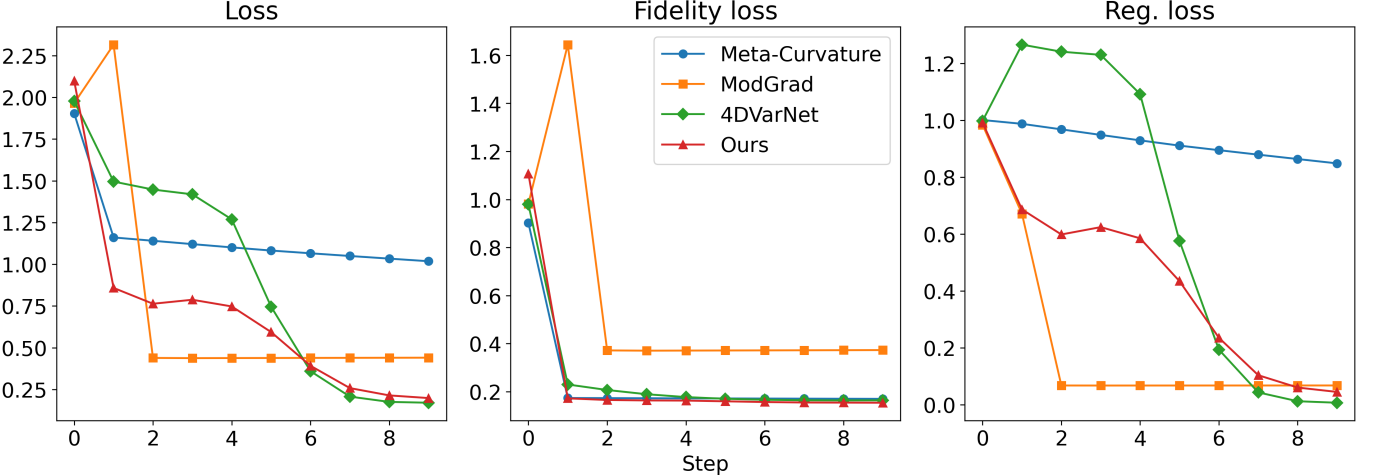


Fig. 2: Curve of the lower-level cost function on validation data: total loss (loss), loss of data fidelity term (fidelity loss), and loss of regularization term (reg. loss).

VI. APPLICATION: ESI PROBLEM

A. Problem: EEG source imaging (ESI)

As an application for the method proposed in this paper, we focus on the inverse problem appearing in ESI. Electroencephalography (EEG) is a technique in which the electric potentials caused by the electrical activity of the brain are measured at the scalp using an array of electrodes. The relation between the scalp measurements and the brain activity is typically modeled as in Eq(1) where $\mathbf{Y} \in \mathbb{R}^{n \times t}$ contains the potential readings at the n electrodes and t instants, $\mathbf{X} \in \mathbb{R}^{s \times t}$ contains the coefficients of the s electric dipoles that model different clusters of neurons at each instant, and $\varepsilon \in \mathbb{R}^{n \times t}$ represents the measurement noise or any other distortion that may impact the EEG signals. The leadfield matrix $\mathbf{L} \in \mathbb{R}^{n \times s}$ relates the relationship between the s source current dipoles (typically placed on the cortex) and the electric potentials they generate at the n electrodes. It is computed using numerical methods such as the finite element method (FEM) or the boundary element method (BEM) [45]. Recovering the source activity from the EEG measurements is an ill-posed inverse problem due to the dimensions and ill-conditioning of \mathbf{L} .

B. Data simulation

a) *Head model and forward operator:* All experiments rely on synthetic EEG data in order to ensure the availability of ground-truth source activity and enable quantitative evaluation of the inverse solutions. A common head model and forward operator are used for all datasets. The head model is based on the *fsaverage* MRI template from FreeSurfer, with the cortical surface subsampled into 994 source locations, following the protocol described in [46]. EEG measurements are simulated using the *standard_1020* electrode montage with 90 sensors provided by MNE-Python [47].

The leadfield matrix $\mathbf{L} \in \mathbb{R}^{90 \times 994}$ is computed using BEM with three compartments (brain, skull, and scalp) and conductivity values (0.3, 0.006, 0.3) S m^{-2} . This forward model is shared across all simulation settings, while the source temporal dynamics are generated using two different approaches described below.

b) *SEREEGA-based simulations:* The first dataset is generated using the SEREEGA toolbox [48], following simulation protocols commonly used in learning-based ESI studies [46]. Source activity consists of single extended cortical sources with Gaussian temporal waveforms. For each sample, a spatially contiguous source patch is formed by aggregating neighboring dipoles around a randomly selected seed, with amplitudes decreasing as a function of geodesic distance. Temporal waveforms follow the Gaussian parametrization implemented in SEREEGA, with parameters drawn from uniform distributions as defined in [49]. Each simulated signal contains 64 time samples. A total of 10,000 samples are generated and split into training and validation sets using an 80%/20% ratio.

c) *Neural mass model simulations:* To evaluate the proposed method under more realistic and nonlinear source dynamics, a second dataset is generated using a neural mass model (NMM) framework, following the simulation setup described in [50]. In this setting, cortical activity is generated by coupled neural population models, producing physiologically plausible oscillatory signals through nonlinear interactions between excitatory and inhibitory subpopulations.

Spatial source configurations are generated in the same manner as in the SEREEGA dataset, using localized extended patches of neighboring dipoles, ensuring consistent spatial characteristics across datasets. In contrast to the Gaussian waveforms used in SEREEGA, temporal dynamics are governed by the underlying NMM equations, resulting in more complex, nonstationary

time courses. Each simulated signal contains 500 time samples. As with the SEREEGA dataset, 10,000 samples are generated and split into training and validation sets using an 80%/20% ratio.

Together, these two datasets provide complementary testbeds for evaluating the proposed learned MM solver: SEREEGA offers a standardized benchmark with controlled temporal structure, while the NMM simulations probe performance under biologically plausible and highly nonlinear dynamics.

C. Algorithm configuration

To ensure consistent conditions across solver experiments, we configure the algorithm as follows. The upper-level problem can in principle be optimized using any standard gradient-based optimizer commonly employed for training neural networks. In our experiments, we use ADAM for 500 epochs with a learning rate of 5×10^{-5} , while all other hyperparameters are set to their default values in PyTorch. The upper-level loss function is:

$$\ell(\mathbf{X}, \hat{\mathbf{X}}) = S_C(\mathbf{X}, \hat{\mathbf{X}}) + S_C(\mathbf{X}, \Phi(\mathbf{X}; \boldsymbol{\theta})). \quad (12)$$

In the lower-level problem, choosing the number of iterations I is critical: larger I improves accuracy but increases computational cost, while smaller I may be insufficient for convergence. Empirically, we found $I = 10$ to be a good trade-off. To further demonstrate stability, we initialize $\mathbf{X}^0 \sim 10^{-3} \mathcal{N}(0, 1)$, where $\mathcal{N}(0, 1)$ is the standard Gaussian. Finally, the lower-level loss is also defined using cosine similarity:

$$u(\mathbf{X}; \mathbf{Y}, \boldsymbol{\theta}) = S_C(\mathbf{X}, \mathbf{LX}) + S_C(\mathbf{X}, \Phi(\mathbf{X}; \boldsymbol{\theta})). \quad (13)$$

VII. EVALUATION

A. Evaluation metrics

Following [49], we use five metrics to evaluate the performance of the algorithm on the ESI task: the localization error (LE), the area under the ROC curve (AUC), the normalized mean squared error (nMSE), the peak signal to noise ratio (PSNR) and the time error (TE). The LE indicates how well the method can localize the active source. The AUC is used to quantify the ability to estimate the source extension. The nMSE and PSNR are used to evaluate amplitude reconstruction, and the TE measures the ability of the method to reconstruct the waveform precisely.

B. Results

We compare the proposed approach with representative baselines drawn from two related families of methods: Meta-Curvature [13] and ModGrad [14] implement learned gradient transformations within the MAML framework [15], while 4DVarNet [3] represents a learning-to-learn variational solver and serves as a strong reference point for our development.²

Table I reports quantitative results under four training–evaluation configurations: (i) in-domain evaluation on SEREEGA, (ii) in-domain evaluation on NMM, (iii) cross-dataset generalization from SEREEGA to NMM, and (iv) the reverse setting from NMM to SEREEGA. These experiments assess not only reconstruction accuracy but also robustness to shifts in temporal dynamics and data generation models.

a) In-domain performance: In this context, the proposed method consistently achieves the best overall performance across all metrics. On SEREEGA, our approach substantially improves localization error (LE) and normalized MSE, while yielding higher PSNR and AUC than all baselines. On the more challenging NMM dataset, which features nonlinear and nonstationary temporal dynamics, our method again delivers the lowest LE and nMSE, as well as the highest PSNR. Although Meta-Curvature attains a slightly higher AUC in this setting, it does so at the cost of significantly larger temporal error (TE), whereas our method achieves a more favorable accuracy–stability trade-off.

b) Cross-dataset generalization: Cross-dataset evaluation reveals a more pronounced separation between methods. When trained on SEREEGA and evaluated on NMM, as well as in the reverse configuration, the proposed solver consistently outperforms 4DVarNet across all reported metrics. In particular, we observe clear gains in LE, nMSE, and PSNR, indicating that the learned MM-based curvature model generalizes more robustly across datasets with different temporal resolutions and underlying generative processes. These results highlight the ability of the proposed approach to capture transferable optimization geometry, rather than overfitting to dataset-specific temporal statistics.

Meta-Curvature and ModGrad are not included in the cross-dataset experiments. Both methods rely on learned update rules that are intrinsically tied to a fixed temporal dimensionality, which prevents their direct application when the temporal resolution differs between training and evaluation data. This limitation further emphasizes the advantage of the proposed formulation, whose MM-based structure remains agnostic to temporal length and naturally accommodates variable sequence dimensions.

²For Meta-Curvature and ModGrad, we reuse the architectures of their learned preconditioners and integrate them into a standard gradient-descent scheme, with careful hyperparameter tuning to ensure competitive performance.

c) *Discussion:* Across all evaluation scenarios, the proposed learned MM solver demonstrates a consistent advantage in terms of accuracy, robustness, and stability. The strong cross-dataset performance suggests that learning a structured curvature majorant, rather than a full update rule, yields better generalization in ill-posed inverse problems. Overall, these results confirm that the proposed approach combines the empirical effectiveness of learned optimization with the theoretical robustness of MM, establishing a favorable trade-off between performance and reliability.

VIII. CONCLUSION

In this work, we introduced a learned MM framework for solving ill-posed inverse problems within a bilevel optimization setting. Rather than learning a full optimizer or unrolled update rule, our approach learns a structured curvature majorant that governs each MM step, while rigorously preserving the descent guarantees of classical MM algorithms. The majorant is parameterized by a lightweight recurrent architecture that adapts to the current iterate and its gradient, thereby combining the transparency and stability of surrogate-based optimization with the flexibility of data-driven learning.

From a theoretical standpoint, we derived explicit curvature bounds for cosine-similarity losses, leading to simple diagonal quadratic majorants and valid MM updates even in the presence of nonlinear learned representations. When closed-form bounds are unavailable, we proposed an automatic curvature estimation strategy based on power iteration and HVPs, enabling the construction of valid MM majorants for complex losses and architectures. Together, these results yield a provably convergent lower-level solver and guarantee convergence to stationary points within the bilevel learning framework.

Experimental results on ESI demonstrate that the proposed method consistently outperforms deep-unrolled and meta-learning baselines in terms of localization accuracy, reconstruction quality, and robustness. In particular, the learned MM solver exhibits strong cross-dataset generalization across simulation settings with markedly different temporal dynamics, highlighting the benefit of learning transferable curvature models rather than dataset-specific update rules.

The proposed framework is general and applicable beyond ESI, extending naturally to other inverse problems. By coupling the learned MM solver with task-adapted regularization or representations, it provides a principled and transferable approach to solving a broad class of ill-posed inverse problems.

REFERENCES

- [1] H. W. Engl, M. Hanke, and A. Neubauer, *Regularization of inverse problems*. Springer Science & Business Media, 1996, vol. 375.
- [2] M. Lustig, D. L. Donoho, J. M. Santos, and J. M. Pauly, “Compressed sensing mri,” *IEEE Signal Processing Magazine*, vol. 25, no. 2, pp. 72–82, 2008.
- [3] R. Fablet, B. Chapron, L. Drumetz, E. Mémin, O. Pannekoucke, and F. Rousseau, “Learning variational data assimilation models and solvers,” *Journal of Advances in Modeling Earth Systems*, vol. 13, no. 10, p. e2021MS002572, 2021, e2021MS002572 2021MS002572.
- [4] R. Grech, T. Cassar, J. Muscat, K. P. Camilleri, S. G. Fabri, M. Zervakis, P. Xanthopoulos, V. Sakkalis, and B. Vanrumste, “Review on solving the inverse problem in eeg source analysis,” *Journal of neuroengineering and rehabilitation*, vol. 5, pp. 1–33, 2008.
- [5] K. Gregor and Y. LeCun, “Learning fast approximations of sparse coding,” in *Proceedings of the 27th international conference on international conference on machine learning*, 2010, pp. 399–406.
- [6] Y. Yang, J. Sun, H. Li, and Z. Xu, “Deep admm-net for compressive sensing mri,” in *Advances in Neural Information Processing Systems*, vol. 29. Curran Associates, Inc., 2016.
- [7] J. Adler and O. Öktem, “Learned primal-dual reconstruction,” *IEEE Transactions on Medical Imaging*, vol. 37, no. 6, pp. 1322–1332, 2018.
- [8] J. Liu, X. Chen, Z. Wang, and W. Yin, “Alista: Analytic weights are as good as learned weights in lista,” in *International conference on learning representations*, 2019.
- [9] S. Arridge, P. Maass, O. Öktem, and C.-B. Schönlieb, “Solving inverse problems using data-driven models,” *Acta Numerica*, vol. 28, pp. 1–174, 2019.
- [10] V. Monga, Y. Li, and Y. C. Eldar, “Algorithm unrolling: Interpretable, efficient deep learning for signal and image processing,” *IEEE Signal Processing Magazine*, vol. 38, no. 2, pp. 18–44, 2021.
- [11] M. Andrychowicz, M. Denil, S. G. Colmenarejo, M. W. Hoffman, D. Pfau, T. Schaul, B. Shillingford, and N. de Freitas, “Learning to learn by gradient descent by gradient descent,” in *Proceedings of the 30th International Conference on Neural Information Processing Systems*, ser. NIPS’16. Red Hook, NY, USA: Curran Associates Inc., 2016, p. 3988–3996.
- [12] O. Wichrowska, N. Maheswaranathan, M. W. Hoffman, S. G. Colmenarejo, M. Denil, N. de Freitas, and J. Sohl-Dickstein, “Learned optimizers that scale and generalize,” in *International Conference on Machine Learning*. PMLR, 2017, pp. 3751–3760.
- [13] E. Park and J. B. Oliva, “Meta-curvature,” in *Advances in Neural Information Processing Systems (NeurIPS)*, vol. 32, 2019.
- [14] C. Simon, P. Koniusz, R. Nock, and M. Harandi, “On modulating the gradient for meta-learning,” in *The European Conference on Computer Vision*. Cham: Springer International Publishing, 2020, pp. 556–572.
- [15] C. Finn, P. Abbeel, and S. Levine, “Model-agnostic meta-learning for fast adaptation of deep networks,” in *Proceedings of the 34th International Conference on Machine Learning - Volume 70*, ser. ICML’17. JMLR.org, 2017, p. 1126–1135.
- [16] D. R. Hunter, K. Lange, and I. Yang, “Optimization transfer using surrogate objective functions,” *Journal of Computational and Graphical Statistics*, vol. 9, no. 1, pp. 1–20, 2000.
- [17] S. Ghadimi and M. Wang, “Approximation methods for bilevel programming,” 2018.
- [18] K. Ji, J. Yang, and Y. Liang, “Bilevel optimization: Convergence analysis and enhanced design,” in *Proceedings of the 38th International Conference on Machine Learning*, ser. Proceedings of Machine Learning Research, vol. 139. PMLR, 18–24 Jul 2021, pp. 4882–4892.
- [19] A. P. Dempster, N. M. Laird, and D. B. Rubin, “Maximum likelihood from incomplete data via the EM algorithm,” *Journal of the Royal Statistical Society: Series B (Methodological)*, vol. 39, no. 1, pp. 1–38, 1977.
- [20] I. Daubechies, R. DeVore, M. Fornasier, and C. S. Güntürk, “Iteratively reweighted least squares minimization for sparse recovery,” *Communications on Pure and Applied Mathematics*, vol. 63, no. 1, pp. 1–38, 2010.
- [21] D. Geman and G. Reynolds, “Constrained restoration and the recovery of discontinuities,” *IEEE Transactions on Pattern Analysis and Machine Intelligence*, vol. 14, no. 3, pp. 367–383, 1992.
- [22] M. A. T. Figueiredo, R. D. Nowak, and S. J. Wright, “Gradient projection for sparse reconstruction: Application to compressed sensing and other inverse problems,” *IEEE Journal of Selected Topics in Signal Processing*, vol. 1, no. 4, pp. 586–597, 2007.
- [23] Y. Saad, *Iterative Methods for Sparse Linear Systems*. SIAM, 2003.
- [24] M. Benzi, “Preconditioning techniques for large linear systems: a survey,” *Journal of Computational Physics*, vol. 182, no. 2, pp. 418–477, 2002.

[25] J. Nocedal and S. J. Wright, *Numerical Optimization*, 2nd ed. Springer, 2006.

[26] J. Duchi, E. Hazan, and Y. Singer, “Adaptive subgradient methods for online learning and stochastic optimization,” *Journal of Machine Learning Research*, vol. 12, no. 61, pp. 2121–2159, 2011.

[27] D. P. Kingma and J. Ba, “Adam: A method for stochastic optimization,” 2015.

[28] P. Fahy, M. Golbabaei, and M. J. Ehrhardt, “Greedy learning to optimize with convergence guarantees,” *arXiv preprint arXiv:2406.00260*, 2024.

[29] E. Gärtner, L. Metz, M. Andriluka, C. D. Freeman, and C. Sminchisescu, “Transformer-based learned optimization,” in *2023 IEEE/CVF Conference on Computer Vision and Pattern Recognition*, 2023, pp. 11 970–11 979.

[30] S. V. Venkatakrishnan, C. A. Bouman, and B. Wohlberg, “Plug-and-play priors for model based reconstruction,” in *2013 IEEE Global Conference on Signal and Information Processing*, 2013, pp. 945–948.

[31] S. Diamond, V. Sitzmann, F. Heide, and G. Wetzstein, “Unrolled optimization with deep priors,” *arXiv preprint arXiv:1705.08041*, 2017.

[32] Y. Romano, M. Elad, and P. Milanfar, “The little engine that could: Regularization by denoising (red),” *SIAM Journal on Imaging Sciences*, vol. 10, no. 4, pp. 1804–1844, 2017.

[33] E. T. Reehorst and P. Schniter, “Regularization by denoising: Clarifications and new interpretations,” *IEEE Transactions on Computational Imaging*, vol. 5, no. 1, pp. 52–67, 2019.

[34] B. Xin, T. Phan, L. Axel, and D. Metaxas, “Learned half-quadratic splitting network for mr image reconstruction,” in *Proceedings of The 5th International Conference on Medical Imaging with Deep Learning*, ser. Proceedings of Machine Learning Research, vol. 172. PMLR, 06–08 Jul 2022, pp. 1403–1412.

[35] C. R. Vogel, *Computational Methods for Inverse Problems*, ser. Frontiers in Applied Mathematics. SIAM, 2002, vol. 23.

[36] H. Antil, Z. W. Di, and R. Khatri, “Bilevel optimization, deep learning and fractional laplacian regularization with applications in tomography,” *Inverse Problems*, vol. 36, no. 6, p. 064001, 2020.

[37] S. Boyd and L. Vandenberghe, *Convex Optimization*. Cambridge University Press, 2004.

[38] Y. Nesterov, *Introductory Lectures on Convex Optimization: A Basic Course*. Springer, 2004.

[39] M. Q. Pham, J. E. Cohen, and T. Chonavel, “A second-order majorant algorithm for nonnegative matrix factorization,” 2025, preprint.

[40] B. A. Pearlmutter, “Fast exact multiplication by the hessian,” *Neural Computation*, vol. 6, no. 1, pp. 147–160, 01 1994.

[41] G. H. Golub and C. F. Van Loan, *Matrix Computations - 4th Edition*. Philadelphia, PA: Johns Hopkins University Press, 2013.

[42] C. Crockett, J. A. Fessler *et al.*, “Bilevel methods for image reconstruction,” *Foundations and Trends® in Signal Processing*, vol. 15, no. 2-3, pp. 121–289, 2022.

[43] L. Franceschi, P. Frasconi, S. Salzo, R. Grazi, and M. Pontil, “Bilevel programming for hyperparameter optimization and meta-learning,” *Journal of Machine Learning Research*, vol. 21, no. 194, pp. 1–36, 2020.

[44] X. Shi, Z. Chen, H. Wang, D.-Y. Yeung, W.-k. Wong, and W.-c. Woo, “Convolutional lstm network: a machine learning approach for precipitation nowcasting,” in *Proceedings of the 29th International Conference on Neural Information Processing Systems - Volume 1*, ser. NIPS’15. Cambridge, MA, USA: MIT Press, 2015, p. 802–810.

[45] J. Kybic, M. Clerc, T. Abboud, O. Faugeras, R. Keriven, and T. Papadopoulou, “A common formalism for the integral formulations of the forward eeg problem,” *IEEE transactions on medical imaging*, vol. 24, no. 1, pp. 12–28, 2005.

[46] R. Sun, A. Sohrabpour, G. A. Worrell, and B. He, “Deep neural networks constrained by neural mass models improve electrophysiological source imaging of spatiotemporal brain dynamics,” *Proceedings of the National Academy of Sciences*, vol. 119, no. 31, p. e2201128119, 2022.

[47] A. Gramfort, M. Luessi, E. Larson, D. A. Engemann, D. Strohmeier, C. Brodbeck, R. Goj, M. Jas, T. Brooks, L. Parkkonen, and M. S. Hämäläinen, “MEG and EEG data analysis with MNE-Python,” *Frontiers in Neuroscience*, vol. 7, no. 267, pp. 1–13, 2013.

[48] L. R. Krol, J. Pawlitzki, F. Lotte, K. Gramann, and T. O. Zander, “Sereega: Simulating event-related eeg activity,” *Journal of neuroscience methods*, vol. 309, pp. 13–24, 2018.

[49] S. Reynaud, A. Merlini, D. Ben Salem, and F. Rousseau, “Comprehensive analysis of supervised learning methods for electrical source imaging,” *Frontiers in Neuroscience*, vol. 18, p. 1444935, 2024.

[50] S. Reynaud, “Machine learning for inverse problem resolution to study brain electrophysiological activity,” Theses, Ecole nationale supérieure Mines-Télécom Atlantique, Sep. 2025.

APPENDIX A PROOF OF BOUNDEDNESS OF THE OBJECTIVE FUNCTION

This appendix provides the proof that the lower objective function (13) used in the ESI is bounded and satisfies the smoothness conditions. We first establish the boundedness of each term, then derive spectral bounds for the Jacobian and Hessian of the learned regularizer $\Phi_\theta(\mathbf{x})$, and finally conclude the boundedness of the total loss.

General Bound for the Derivative of a Ratio Form

The following lemma will be useful in the proof of Proposition 1.

Lemma 1. *Let $a, b : \mathbb{R}^s \rightarrow \mathbb{R}$ be twice continuously differentiable with $b(\mathbf{x}) \neq 0$ for all $\mathbf{x} \in \mathbb{R}^s$. Define $\xi(\mathbf{x}) = \frac{a(\mathbf{x})}{b(\mathbf{x})}$. Then, for all $\mathbf{x} \in \mathbb{R}^s$, $\|\nabla^2 \xi(\mathbf{x})\| \leq \sum_{i=1}^4 \kappa_i(\mathbf{x})$, where*

$$\begin{aligned}\kappa_1(\mathbf{x}) &= \frac{1}{b(\mathbf{x})} \|\nabla^2 a(\mathbf{x})\|, \kappa_2(\mathbf{x}) = \frac{|a(\mathbf{x})|}{b(\mathbf{x})^2} \|\nabla^2 b(\mathbf{x})\| \\ \kappa_3(\mathbf{x}) &= \frac{2}{b(\mathbf{x})^2} \|\nabla a(\mathbf{x})^\top \nabla b(\mathbf{x})\|, \kappa_4(\mathbf{x}) = 2 \frac{|a(\mathbf{x})|}{b(\mathbf{x})^3} \|\nabla b(\mathbf{x})\|^2.\end{aligned}$$

Proof. We compute the first and second derivatives of ξ at $\mathbf{x} \in \mathbb{R}^s$:

$$\begin{aligned}\nabla \xi(\mathbf{x}) &= \frac{1}{b(\mathbf{x})} \nabla a(\mathbf{x}) - \frac{a(\mathbf{x})}{b(\mathbf{x})^2} \nabla b(\mathbf{x}), \\ \nabla^2 \xi(\mathbf{x}) &= \frac{1}{b(\mathbf{x})} \nabla^2 a(\mathbf{x}) - \frac{1}{b(\mathbf{x})^2} \nabla a(\mathbf{x}) \nabla b(\mathbf{x})^\top \\ &\quad - \frac{1}{b(\mathbf{x})^2} (a(\mathbf{x}) \nabla^2 b(\mathbf{x}) + \nabla b(\mathbf{x}) \nabla a(\mathbf{x})^\top) \\ &\quad + \frac{2a(\mathbf{x})}{b(\mathbf{x})^3} \nabla b(\mathbf{x}) \nabla b(\mathbf{x})^\top \\ &= -\frac{1}{b(\mathbf{x})^2} (\nabla a(\mathbf{x}) \nabla b(\mathbf{x})^\top + \nabla b(\mathbf{x}) \nabla a(\mathbf{x})^\top) \\ &\quad + \frac{1}{b(\mathbf{x})} \nabla^2 a(\mathbf{x}) - \frac{a(\mathbf{x})}{b(\mathbf{x})^2} \nabla^2 b(\mathbf{x}) \\ &\quad + 2 \frac{a(\mathbf{x})}{b(\mathbf{x})^3} \nabla b(\mathbf{x}) \nabla b(\mathbf{x})^\top.\end{aligned}$$

This concludes the proof. \square

Based on these derivative expressions, we now derive upper bounds for the Hessian of two cases: $S_C(\mathbf{Lx}, \mathbf{y})$ and $S_C(\Phi_{\boldsymbol{\theta}}(\mathbf{x}), (\mathbf{x}))$;

1. Upper bound of $\nabla^2 S_C(\mathbf{Lx}, \mathbf{y})$: We set $a(\mathbf{x}) = \mathbf{y}^\top \mathbf{Lx}$ and $b(\mathbf{x}) = \|\mathbf{y}\| \|\mathbf{Lx}\|$ for $\mathbf{x} \in \mathcal{C}, \mathbf{y} \in \mathbb{R}^{*n}$. Now we compute the first and second derivatives of $a(\mathbf{x})$ and $b(\mathbf{x})$,

$$\begin{aligned}\nabla a(\mathbf{x}) &= \mathbf{L}^\top \mathbf{y}, \\ \nabla^2 a(\mathbf{x}) &= 0, \\ \nabla b(\mathbf{x}) &= \|\mathbf{y}\| \frac{\mathbf{L}^\top \mathbf{Lx}}{\|\mathbf{Lx}\|}, \\ \nabla^2 b(\mathbf{x}) &= \|\mathbf{y}\| \left(\frac{1}{\|\mathbf{Lx}\|} \mathbf{L}^\top \mathbf{L} - \frac{1}{\|\mathbf{Lx}\|^3} \mathbf{L}^\top \mathbf{Lx} \mathbf{x}^\top \mathbf{L}^\top \mathbf{L} \right)\end{aligned}$$

We recall that, for all $\mathbf{x} \in \mathcal{C}$ such that $\mathbf{Lx} \neq 0$ and $\mathbf{y} \neq 0$, the cosine similarity can be written as the ratio

$$S_C(\mathbf{Lx}, \mathbf{y}) = \frac{a(\mathbf{x})}{b(\mathbf{x})}.$$

Therefore, we can apply Lemma 1 to the map $\mathbf{x} \mapsto \frac{a(\mathbf{x})}{b(\mathbf{x})}$, where the terms $\kappa_i(\mathbf{x})$ collect the contributions of ∇a , $\nabla^2 a$, ∇b , and $\nabla^2 b$ to the Hessian. Since $\nabla^2 a(\mathbf{x}) = 0$, the corresponding contribution vanishes, and we only need to bound the remaining terms.

First, using the expression of $\nabla^2 b(\mathbf{x})$ together with standard norm inequalities and the fact that

$$\left\| \mathbf{I} - \frac{1}{\|\mathbf{Lx}\|^2} \mathbf{Lx} \mathbf{x}^\top \mathbf{L}^\top \right\| \leq 1$$

(because this matrix is an orthogonal projector), we obtain

$$\begin{aligned}\kappa_2(\mathbf{x}) &\leq \frac{|\mathbf{y}^\top \mathbf{Lx}|}{(\|\mathbf{Lx}\| \|\mathbf{y}\|)^2} \|\mathbf{y}\| \frac{\|\mathbf{L}\|^2}{\|\mathbf{Lx}\|} \left\| \mathbf{I} - \frac{1}{\|\mathbf{Lx}\|^2} \mathbf{Lx} \mathbf{x}^\top \mathbf{L}^\top \right\| \\ &\leq \frac{\|\mathbf{L}\|^2}{\|\mathbf{Lx}\|^2}\end{aligned}\tag{14}$$

where we used $|\mathbf{y}^\top \mathbf{Lx}| \leq \|\mathbf{y}\| \|\mathbf{Lx}\|$.

Similarly, by bounding the mixed terms that involve $\nabla a(\mathbf{x})$ and $\nabla b(\mathbf{x})$ with Cauchy–Schwarz and $\|\mathbf{L}^\top \mathbf{L}\| \leq \|\mathbf{L}\|^2$, we obtain

$$\kappa_3(\mathbf{x}) \leq \frac{2}{\|\mathbf{Lx}\|^2 \|\mathbf{y}\|^2} \frac{\|\mathbf{y}\|}{\|\mathbf{Lx}\|} \|\mathbf{y}^\top \mathbf{L} \mathbf{L}^\top \mathbf{Lx}\| \leq 2 \frac{\|\mathbf{L}\|^2}{\|\mathbf{Lx}\|^2}\tag{15}$$

and, for the remaining quadratic term in $\nabla b(\mathbf{x})$, we get

$$\kappa_4(\mathbf{x}) \leq 2 \frac{|\mathbf{y}^\top \mathbf{Lx}|}{\|\mathbf{Lx}\|^3 \|\mathbf{y}\|^3} \frac{\|\mathbf{y}\|^2}{\|\mathbf{Lx}\|^2} \|\mathbf{L}^\top \mathbf{Lx}\|^2 \leq 2 \frac{\|\mathbf{L}\|^2}{\|\mathbf{Lx}\|^2}\tag{16}$$

where again we used $|\mathbf{y}^\top \mathbf{L}\mathbf{x}| \leq \|\mathbf{y}\| \|\mathbf{L}\mathbf{x}\|$ and $\|\mathbf{L}^\top \mathbf{L}\mathbf{x}\| \leq \|\mathbf{L}\|^2 \|\mathbf{x}\|$ together with the normalization coming from $b(\mathbf{x})$.

Using Lemma 1 and Equations (14), (15), and (16) we get

$$\|\nabla^2 S_C(\mathbf{L}\mathbf{x}, \mathbf{y})\| \leq 5 \frac{\|\mathbf{L}\|^2}{\|\mathbf{L}\mathbf{x}\|^2} \leq \frac{5}{\delta^2} \|\mathbf{L}\|^2, \quad \forall \mathbf{x} \in \mathcal{C}$$

where, in the last inequality, we used the assumption that there exists $\delta > 0$ such that $\|\mathbf{L}\mathbf{x}\| \geq \delta$ for all $\mathbf{x} \in \mathcal{C}$. \square

2. Upper bound of $\nabla^2 h(\Phi(\mathbf{x}; \boldsymbol{\theta})) = S_C(\Phi(\mathbf{x}; \boldsymbol{\theta}), \mathbf{x})$: We now consider the cosine similarity between the output of an autoencoder $\Phi : \mathbb{R}^s \rightarrow \mathbb{R}^s$ and its input. Let

$$\mathbf{J}_\mathbf{x}(\mathbf{x}; \boldsymbol{\theta}) = \nabla_{\mathbf{x}} \Phi(\mathbf{x}; \boldsymbol{\theta}) \in \mathbb{R}^{s \times s}$$

be the Jacobian of the autoencoder. Now set $a(\mathbf{x}) = \Phi(\mathbf{x}; \boldsymbol{\theta})^\top \mathbf{x}$ and $b(\mathbf{x}) = \|\Phi(\mathbf{x}; \boldsymbol{\theta})\| \|\mathbf{x}\|$. The gradient and hessian of $a(\mathbf{x})$ with respect to \mathbf{x} can be written as

$$\nabla_{\mathbf{x}} a(\mathbf{x}) = \mathbf{J}_\mathbf{x}(\mathbf{x}; \boldsymbol{\theta})^\top \mathbf{x} + \Phi(\mathbf{x}; \boldsymbol{\theta}),$$

and

$$\nabla_{\mathbf{x}}^2 a(\mathbf{x}) = \mathbf{J}_\mathbf{x}(\mathbf{x}; \boldsymbol{\theta}) + \mathbf{J}_\mathbf{x}(\mathbf{x}; \boldsymbol{\theta})^\top + \sum_{i=1}^s x_i \nabla_{\mathbf{x}}^2 [\Phi(\mathbf{x}; \boldsymbol{\theta})]_i.$$

The gradient and the hessian of $b(\mathbf{x})$ with respect to \mathbf{x} are

$$\nabla_{\mathbf{x}} b(\mathbf{x}) = \|\mathbf{x}\| \nabla_{\mathbf{x}} \|\Phi(\mathbf{x}; \boldsymbol{\theta})\| + \|\Phi(\mathbf{x}; \boldsymbol{\theta})\| \nabla_{\mathbf{x}} \|\mathbf{x}\|,$$

and

$$\begin{aligned} \nabla_{\mathbf{x}}^2 b(\mathbf{x}) &= \nabla_{\mathbf{x}} \|\Phi(\mathbf{x}; \boldsymbol{\theta})\| \nabla_{\mathbf{x}} \|\mathbf{x}\|^\top + \|\mathbf{x}\| \nabla_{\mathbf{x}}^2 \|\Phi(\mathbf{x}; \boldsymbol{\theta})\| \\ &\quad + \nabla_{\mathbf{x}} \|\mathbf{x}\| \nabla_{\mathbf{x}} \|\Phi(\mathbf{x}; \boldsymbol{\theta})\|^\top + \|\Phi(\mathbf{x}; \boldsymbol{\theta})\| \nabla_{\mathbf{x}}^2 \|\mathbf{x}\| \end{aligned}$$

where

$$\begin{aligned} \nabla_{\mathbf{x}} \|\mathbf{x}\| &= \frac{\mathbf{x}}{\|\mathbf{x}\|}, \quad \nabla_{\mathbf{x}}^2 \|\mathbf{x}\| = \frac{1}{\|\mathbf{x}\|} \left(\mathbf{I} - \frac{\mathbf{x}\mathbf{x}^\top}{\|\mathbf{x}\|^2} \right), \\ \nabla_{\mathbf{x}} \|\Phi(\mathbf{x}; \boldsymbol{\theta})\| &= \frac{1}{\|\Phi(\mathbf{x}; \boldsymbol{\theta})\|} \mathbf{J}_\mathbf{x}(\mathbf{x}; \boldsymbol{\theta})^\top \Phi(\mathbf{x}; \boldsymbol{\theta}), \\ \nabla_{\mathbf{x}}^2 \|\Phi(\mathbf{x}; \boldsymbol{\theta})\| &= \mathbf{J}_\mathbf{x}(\mathbf{x}; \boldsymbol{\theta})^\top \left(\frac{\mathbf{I}}{\|\Phi(\mathbf{x}; \boldsymbol{\theta})\|} - \frac{\Phi(\mathbf{x}; \boldsymbol{\theta}) \Phi(\mathbf{x}; \boldsymbol{\theta})^\top}{\|\Phi(\mathbf{x}; \boldsymbol{\theta})\|^3} \right) \\ &\quad \mathbf{J}_\mathbf{x}(\mathbf{x}; \boldsymbol{\theta}) + \sum_{i=1}^s \frac{\Phi_i(\mathbf{x}; \boldsymbol{\theta})}{\|\Phi(\mathbf{x}; \boldsymbol{\theta})\|} \nabla_{\mathbf{x}}^2 [\Phi(\mathbf{x}; \boldsymbol{\theta})]_i. \end{aligned}$$

Then their sup norm are

$$\begin{aligned} \|\nabla_{\mathbf{x}} \|\mathbf{x}\|\| &\leq 1, \quad \|\nabla_{\mathbf{x}}^2 \|\mathbf{x}\|\| \leq \frac{1}{\|\mathbf{x}\|}, \\ \|\nabla_{\mathbf{x}} \|\Phi(\mathbf{x}; \boldsymbol{\theta})\|\| &\leq \|\mathbf{J}_\mathbf{x}(\mathbf{x}; \boldsymbol{\theta})\|, \\ \|\nabla_{\mathbf{x}}^2 \|\Phi(\mathbf{x}; \boldsymbol{\theta})\|\| &\leq \frac{\|\mathbf{J}_\mathbf{x}(\mathbf{x}; \boldsymbol{\theta})\|^2}{\|\Phi(\mathbf{x}; \boldsymbol{\theta})\|} \\ &\quad + \max_{1 \leq i \leq s} \|\nabla_{\mathbf{x}}^2 [\Phi(\mathbf{x}; \boldsymbol{\theta})]_i\| \frac{\|\Phi(\mathbf{x}; \boldsymbol{\theta})\|_1}{\|\Phi(\mathbf{x}; \boldsymbol{\theta})\|} \\ &\leq \frac{\|\mathbf{J}_\mathbf{x}(\mathbf{x}; \boldsymbol{\theta})\|^2}{\|\Phi(\mathbf{x}; \boldsymbol{\theta})\|} + \alpha \sqrt{s}, \end{aligned}$$

where we denote $\alpha = \max_{1 \leq i \leq s} \|\nabla_{\mathbf{x}}^2 [\Phi(\mathbf{x}; \boldsymbol{\theta})]_i\|$. We now can evaluate the elements which involve in the majoration of $\nabla_{\mathbf{x}} h(\Phi(\mathbf{x}; \boldsymbol{\theta}))$.

$$\begin{aligned} \|\nabla_{\mathbf{x}} a(\mathbf{x})\| &\leq \|\mathbf{J}_{\mathbf{x}}(\mathbf{x}; \boldsymbol{\theta})\| \|\mathbf{x}\| + \|\Phi(\mathbf{x}; \boldsymbol{\theta})\| \\ \|\nabla_{\mathbf{x}} b(\mathbf{x})\| &\leq \|\mathbf{x}\| \|\mathbf{J}_{\mathbf{x}}(\mathbf{x}; \boldsymbol{\theta})\| + \|\Phi(\mathbf{x}; \boldsymbol{\theta})\|, \\ \|\nabla_{\mathbf{x}}^2 a(\mathbf{x})\| &\leq 2\|\mathbf{J}_{\mathbf{x}}(\mathbf{x}; \boldsymbol{\theta})\| + \alpha \|\mathbf{x}\|_1 \\ \|\nabla_{\mathbf{x}}^2 b(\mathbf{x})\| &\leq 2\|\mathbf{J}_{\mathbf{x}}(\mathbf{x}; \boldsymbol{\theta})\| + \frac{\|\Phi(\mathbf{x}; \boldsymbol{\theta})\|}{\|\mathbf{x}\|} \\ &\quad + \|\mathbf{x}\| \left[\frac{\|\mathbf{J}_{\mathbf{x}}(\mathbf{x}; \boldsymbol{\theta})\|}{\|\Phi(\mathbf{x}; \boldsymbol{\theta})\|} + \alpha \sqrt{s} \right] \\ &\leq 3\|\mathbf{J}_{\mathbf{x}}(\mathbf{x}; \boldsymbol{\theta})\| + \alpha \sqrt{s} \|\mathbf{x}\| + 1. \end{aligned}$$

The fusion of all majorations give us the final upper bound of $\nabla_{\mathbf{x}} h(\Phi(\mathbf{x}; \boldsymbol{\theta}))$. \square

APPENDIX B UPPER BOUND FOR AUTOENCODER Φ

We consider the autoencoder mapping defined by the composition of three convolutional layers with SoftReLU nonlinearities:

$$\Phi(\mathbf{x}; \boldsymbol{\theta}) = (\text{Conv} \circ \text{SoftReLU} \circ \text{Conv} \circ \text{SoftReLU} \circ \text{Conv})(\mathbf{x}),$$

which we write explicitly as

$$\begin{aligned} \mathbf{z}_1 &= \mathbf{W}_1 \mathbf{x} + \mathbf{b}_1, & \mathbf{a}_1 &= \sigma(\mathbf{z}_1), \\ \mathbf{z}_2 &= \mathbf{W}_2 \mathbf{a}_1 + \mathbf{b}_2, & \mathbf{a}_2 &= \sigma(\mathbf{z}_2), \\ \mathbf{z}_3 &= \mathbf{W}_3 \mathbf{a}_2 + \mathbf{b}_3. \end{aligned}$$

Then

$$\Phi(\mathbf{x}; \boldsymbol{\theta}) = \mathbf{z}_3, \text{ with } \boldsymbol{\theta} = (\mathbf{W}_1, \mathbf{W}_2, \mathbf{W}_3, \mathbf{b}_1, \mathbf{b}_2, \mathbf{b}_3)$$

We recall that the Soft-ReLU activation σ is given by

$$\begin{aligned} \sigma(\mathbf{z}) &= \frac{1}{2} \left(\mathbf{z} + \sqrt{\mathbf{z}^2 + \varepsilon^2} \right), & \varepsilon > 0, \\ \sigma'(\mathbf{z}) &= \frac{1}{2} \left(1 + \frac{\mathbf{z}}{\sqrt{\mathbf{z}^2 + \varepsilon^2}} \right) \in (0, 1), \\ \sigma''(\mathbf{z}) &= \frac{1}{2} \frac{\varepsilon^2}{(\mathbf{z}^2 + \varepsilon^2)^{3/2}} \leq \frac{1}{2\varepsilon}. \end{aligned}$$

Hence, σ' is uniformly bounded in $(0, 1)$ and σ'' is uniformly bounded by $1/(2\varepsilon)$, independently of \mathbf{z} . These bounds will directly control the Jacobian and Hessian of Φ .

a) *First layer (Conv + SoftReLU):* For the first layer we have

$$\begin{aligned} \mathbf{z}_1 &= \mathbf{W}_1 \mathbf{x} + \mathbf{b}_1, & \mathbf{a}_1 &= \sigma(\mathbf{z}_1) \\ \mathbf{J}(\mathbf{x}; \mathbf{a}_1) &= \text{diag}(\sigma'(\mathbf{z}_1)) \mathbf{W}_1 \\ \nabla^2 a_{1,i}(\mathbf{x}) &= \sigma''(\mathbf{z}_{1,i}) \mathbf{w}_{1,i} \mathbf{w}_{1,i}^\top \end{aligned}$$

where $\mathbf{w}_{1,i}$ denotes the i -th row of \mathbf{W}_1 . Since $\|\text{diag}(\sigma'(\mathbf{z}_1))\| \leq 1$ and $|\sigma''(\mathbf{z}_{1,i})| \leq 1/(2\varepsilon)$, both the Jacobian $\mathbf{J}(\mathbf{x}; \mathbf{a}_1)$ and each Hessian $\nabla^2 a_{1,i}(\mathbf{x})$ are uniformly bounded in \mathbf{x} in terms of $\|\mathbf{W}_1\|$.

b) *Second layer (Conv + SoftReLU):* For the second layer,

$$\begin{aligned} \mathbf{z}_2 &= \mathbf{W}_2 \mathbf{a}_1 + \mathbf{b}_2, & \mathbf{a}_2 &= \sigma(\mathbf{z}_2) \\ \mathbf{J}(\mathbf{x}; \mathbf{a}_2) &= \text{diag}(\sigma'(\mathbf{z}_2)) \mathbf{W}_2 \text{diag}(\sigma'(\mathbf{z}_1)) \mathbf{W}_1 \\ \nabla^2 a_{2,i}(\mathbf{x}) &= \sigma''(\mathbf{z}_{2,i}) (\mathbf{J}(\mathbf{x}; \mathbf{a}_1)^\top \mathbf{w}_{2,i}) (\mathbf{J}(\mathbf{x}; \mathbf{a}_1)^\top \mathbf{w}_{2,i})^\top \\ &\quad + \sigma'(\mathbf{z}_{2,i}) \sum_j w_{2,i,j} \sigma''(\mathbf{z}_{1,j}) \mathbf{w}_{1,j} \mathbf{w}_{1,j}^\top. \end{aligned}$$

Using again that $\|\text{diag}(\sigma'(\cdot))\| \leq 1$ and $|\sigma''(\cdot)| \leq 1/(2\varepsilon)$, together with standard norm inequalities and $\|\mathbf{J}(\mathbf{x}; \mathbf{a}_1)\| \leq \|\mathbf{W}_1\|$, we obtain uniform bounds on both the Jacobian $\mathbf{J}(\mathbf{x}; \mathbf{a}_2)$ and the Hessians $\nabla^2 a_{2,i}(\mathbf{x})$ in terms of $\|\mathbf{W}_1\|$ and $\|\mathbf{W}_2\|$.

c) *Jacobian and Hessian of Φ .*: By composition, the Jacobian of the full mapping Φ is given by

$$\mathbf{J}(\mathbf{x}; \boldsymbol{\theta}) = \mathbf{W}_3 \operatorname{diag}(\sigma'(\mathbf{z}_2)) \mathbf{W}_2 \operatorname{diag}(\sigma'(\mathbf{z}_1)) \mathbf{W}_1$$

$$\text{Therefore, } \|\mathbf{J}(\mathbf{x}; \boldsymbol{\theta})\| \leq \|\mathbf{W}_3\| \|\mathbf{W}_2\| \|\mathbf{W}_1\|$$

where the inequality follows from the submultiplicativity of the operator norm and the fact that $\|\operatorname{diag}(\sigma'(\cdot))\| \leq 1$.

For the Hessian of the i -th output component of Φ , we have

$$\begin{aligned} \nabla_{\mathbf{x}}^2 [\Phi(\mathbf{x}; \boldsymbol{\theta})]_i &= \sum_j w_{3,i,j} \sigma''(\mathbf{z}_{2,j}) \tilde{\mathbf{z}}_1 \tilde{\mathbf{z}}_1^\top \\ &+ \sum_j \sum_k w_{3,i,j} \sigma'(\mathbf{z}_{2,j}) w_{2,j,k} \sigma''(\mathbf{z}_{1,k}) \mathbf{w}_{1,k} \mathbf{w}_{1,k}^\top. \end{aligned}$$

where $\tilde{\mathbf{z}}_1 = \mathbf{W}_1^\top \operatorname{diag}(\sigma'(\mathbf{z}_1)) \mathbf{w}_{2,j}$

Therefore

$$\|\nabla_{\mathbf{x}}^2 [\Phi(\mathbf{x}; \boldsymbol{\theta})]_i\| \leq \frac{1}{2\varepsilon} \|\mathbf{W}_3\| \left(\|\mathbf{W}_1\|^2 \|\mathbf{W}_2\|^2 + \|\mathbf{W}_2\|_1 \|\mathbf{W}_1\|^2 \right).$$

In the last inequality, we use the uniform bound $|\sigma''(\cdot)| \leq 1/(2\varepsilon)$, the bound $\|\operatorname{diag}(\sigma'(\mathbf{z}_1))\| \leq 1$, and standard estimates on the norms of the rank-one matrices appearing in $\nabla_{\mathbf{x}}^2 [\Phi(\mathbf{x}; \boldsymbol{\theta})]_i$, which introduce $\|\mathbf{W}_1\|^2$, $\|\mathbf{W}_2\|^2$ and the ℓ_1 -norm $\|\mathbf{W}_2\|_1$ of \mathbf{W}_2 .

Therefore, both the Jacobian and all component-wise Hessians of Φ are uniformly bounded in \mathbf{x} , with explicit bounds depending only on ε and the layer weight matrices $\mathbf{W}_1, \mathbf{W}_2, \mathbf{W}_3$. This shows that Φ is twice continuously differentiable with bounded first and second derivatives. \square